POLITECNICO DI TORINO
Repository ISTITUZIONALE

On the failure of upscaling the single-collector efficiency to the transport of colloids in an array of collectors

Original
On the failure of upscaling the single-collector efficiency to the transport of colloids in an array of collectors / Messina, Francesca; Tosco, TIZIANA ANNA ELISABETTA; Sethi, Rajandrea. - In: WATER RESOURCES RESEARCH. - ISSN 0043-1397. - STAMPA. - 52:7(2016), pp. 5492-5505. [10.1002/2016WR018592]

Availability:
This version is available at: 11583/2648209 since: 2016-10-20T17:32:49Z

Publisher:
American Geophysical Union

Published
DOI:10.1002/2016WR018592

Terms of use:

This article is made available under terms and conditions as specified in the corresponding bibliographic description in the repository

Publisher copyright

(Article begins on next page)

07 May 2024

AGU PUBLICATIONS

Water Resources Research

RESEARCH ARTICLE
10.1002/2016WR018592

Key Points:
- Numerical simulations were performed in a vertical array of spherical collectors
- Single-collector efficiencies are not uniform along the filter under favorable conditions
- A correlation equation for the upscaled removal efficiency of the entire array is presented

Supporting Information:
- Supporting Information S1

Correspondence to:
R. Sethi,
rajandrea.sethi@polito.it

Citation:
Messina, F., T. Tosco, and R. Sethi (2016), On the failure of upscaling the single-collector efficiency to the transport of colloids in an array of collectors, *Water Resour. Res.*, *52*, 5492–5505, doi:10.1002/2016WR018592.

Received 11 JAN 2016
Accepted 3 JUN 2016
Accepted article online 6 JUN 2016
Published online 22 JUL 2016

© 2016. American Geophysical Union. All Rights Reserved.

On the failure of upscaling the single-collector efficiency to the transport of colloids in an array of collectors

Francesca Messina[1], Tiziana Tosco[1], and Rajandrea Sethi[1]

[1]DIATI, Politecnico di Torino, Torino, Italy

Abstract Defining the removal efficiency of a filter is a key aspect for colloid transport in porous media. Several efforts were devoted to derive accurate correlations for the single-collector removal efficiency, but its upscaling to the entire porous medium is still a challenging topic. A common approach involves the assumption of deposition being independent of the history of transport, that is, the collector efficiency is uniform along the porous medium. However, this approach was shown inadequate under unfavorable deposition conditions. In this work, the authors demonstrate that it is not adequate even in the simplest case of favorable deposition. Computational Fluid Dynamics (CFD) simulations were run in a vertical array of 50 identical spherical collectors. Particle transport was numerically solved by analyzing a broad range of parameters. The results evidenced that when particle deposition is not controlled by Brownian diffusion, nonexponential concentration profiles are retrieved, in contrast with the assumption of uniform efficiency. If sedimentation and interception dominate, the efficiency of the first sphere is significantly higher compared to the others, and then declines along the array down to an asymptotic value. Finally, a correlation for the upscaled removal efficiency of the entire array was derived.

1. Introduction

Colloid transport and deposition in saturated porous media play a significant role in a large number of natural processes and technological applications [*Elimelech et al*., 1998; *Molnar et al*., 2015; *Tien and Payatakes*, 1979], including propagation of microorganisms and pollutants in aquifer systems [*Bianchi Janetti et al*., 2013; *Ngueleu et al*., 2014; *Syngouna and Chrysikopoulos*, 2013; *Torkzaban et al*., 2008], development of novel groundwater remediation technologies based on the injection of micro and nanoparticles [*Saleh et al*., 2005; *Tosco et al*., 2014], use of filters for air, water, and wastewater treatment, in situ recycling of groundwater [*Anders and Chrysikopoulos*, 2005], and applications to enhanced oil recovery [*Zeinijahromi et al*., 2012]. For all these cases, it is of pivotal importance to understand how particles are transported through the porous matrix and how they interact with it [*Tiraferri et al*., 2011; *Torkzaban et al*., 2008], with the final aim of predicting particle removal.

Colloid transport and deposition is a peculiar multiscale problem [*Tosco et al*., 2013]. Colloidal particles suspended in a fluid are transported through the porous medium (typically a granular or fibrous material) and removed by retention onto the filter bed following Brownian diffusion, sedimentation, and interception. As a consequence, the overall macroscale performance of the bed filter, typically quantified through a parameter expressing its removal efficiency [*Cookson*, 1970; *Herzig et al*., 1970], is directly related to pore-scale interactions between particles and the solid matrix. From the macroscale point of view, the problem has been traditionally faced assuming an exponential decay of particle concentration over space, quantified by an empirical first-order removal rate, called filter coefficient [*Iwasaki*, 1937; *McDowell-Boyer et al*., 1986]. On the other hand, mechanistic approaches moved to the microscale to derive the removal efficiency of an individual solid grain (referred to as collector) when immersed in a flow field with particles suspended in it [*Johnson and Hilpert*, 2013; *Li et al*., 2015; *Ma et al*., 2009; *Rajagopalan and Tien*, 1976; *Tufenkji and Elimelech*, 2004; *Yao et al*., 1971]. Several models have been proposed to express the removal efficiency of an isolated sphere as a result of sedimentation, interception, and Brownian diffusion. The impact of the neighboring grains has been included by taking advantage of Happel's sphere-in-cell model, which considers a thin fluid shell surrounding the collector whose thickness is related to the average medium porosity [*Happel*, 1958; *Rajagopalan and Tien*, 1976]. The single-collector models usually assume an additive contribution of the three processes to the overall particle retention [*Yao et al*., 1971].

The removal efficiency of an individual grain, referred to as single-collector removal efficiency, represents the fraction of suspended particles which are removed from the fluid by deposition onto the collector surface [*Yao et al*., 1971], and can be expressed as

$$\eta = 1 - \frac{C_{out}}{C_{in}}, \tag{1}$$

where C_{in} is the flux-averaged concentration of particles in the fluid phase approaching the collector [ML^{-3}] and C_{out} [ML^{-3}] is the flux-averaged concentration downstream the collector. The single-collector removal efficiency η [*Elimelech et al*., 1995; *Petosa et al*., 2010] is obtained as $\eta = \eta_0 \cdot \alpha$, being η_0 the single-collector contact efficiency and α the attachment efficiency, equal to 1 in case of favorable deposition (i.e., in the absence of a repulsive energy barrier between particle and collector), or lower than 1 for unfavorable deposition (i.e., in case an energy barrier exists against deposition). In this work we will consider favorable deposition conditions, hence $\eta = \eta_0$, which will be referred to as "single-collector efficiency."

Even though several correlation equations were developed to predict the single-collector η_0 [*Ma et al*., 2013; *Rajagopalan and Tien*, 1976; *Tufenkji and Elimelech*, 2004; *Yao et al*., 1971], upscaling η_0 to a global removal efficiency E representative of the entire porous medium is still a challenging step. In this sense, *Johnson and Hilpert* [2013] proposed an upscaled efficiency for multiple collectors in the presence of unfavorable deposition conditions. *Long and Hilpert* [2009] also showed that in a random sphere packing, the single-collector efficiency is not uniform because of the local pore geometry and topology in porous media.

Usually, a 3D periodical structure of spheres is adopted as conceptual model for a real porous medium (Figure 1). Vertical sections of the structure may result in arrays of aligned or uneven collectors (see Supporting Information). As a general rule, the removal efficiency of the porous medium results from the combination of the different efficiencies $\eta_{0,i}$ of the collectors encountered along the flow direction. However, the common approach is to assume that the single-collector efficiency of the first sphere η_0 applies to all the subsequent collectors [*Yao*, 1968; *Yao et al*., 1971]. This practical approach is based on the simplifying assumption of complete mixing of the suspension downstream each sphere. However, under several circumstances this assumption may not be adequate, and the use of rigorous CFD simulations must be undertaken in order to determine the concentration distribution after each collector [*Le Borgne et al*., 2011; *Cushman and Ginn*, 2000]. This common approach allows to calculate the actual removal efficiency of each sphere, $\eta_{0,i}$, and consequently the global multiple collector efficiency, E, which defines the capacity of the entire porous medium to retain the particles that pass through it. E can be express as

$$E = 1 - \frac{C}{C_0}, \tag{2}$$

where C_0 and C are, respectively, the flux-averaged concentration of particles entering and exiting the porous medium [ML^{-3}].

For this reason, the vertical array of aligned collectors is adopted in this work as a simplified representation of a porous medium, and CFD simulations of particle transport were performed considering advection, gravity, and Brownian diffusion. Deposition under favorable conditions is controlled by the combined effects of the three transport mechanisms (advection, Brownian diffusion, and gravity) and of the steric effect, due to the finite size of the particles, thus resulting in the 14 removal mechanisms as elucidated by *Messina et al*. [2015]. Among them, the three dominant mechanisms include the combination of advection and Brownian diffusion (AD, usually referred to as Brownian diffusion), the combination of advection and steric effect (AS, usually referred to as interception), and pure gravity (G), as reported in Figure 2. When considering the vertical array of spheres, Figure 2 suggests that the AD mechanism is important for all collectors, while AS and G are relevant only for the first sphere.

Under the assumption of uniform efficiency along the filter, the concentration profiles of both suspended and deposited particles assume an exponential shape. Deviations from exponential profiles have been frequently observed in systems where surface interactions between particles and porous medium, or between suspended and attachment particles, cannot be neglected. In particular, *Johnson and Hilpert* [2013] showed that the common assumption of uniform removal efficiency fails in the presence of repulsive forces

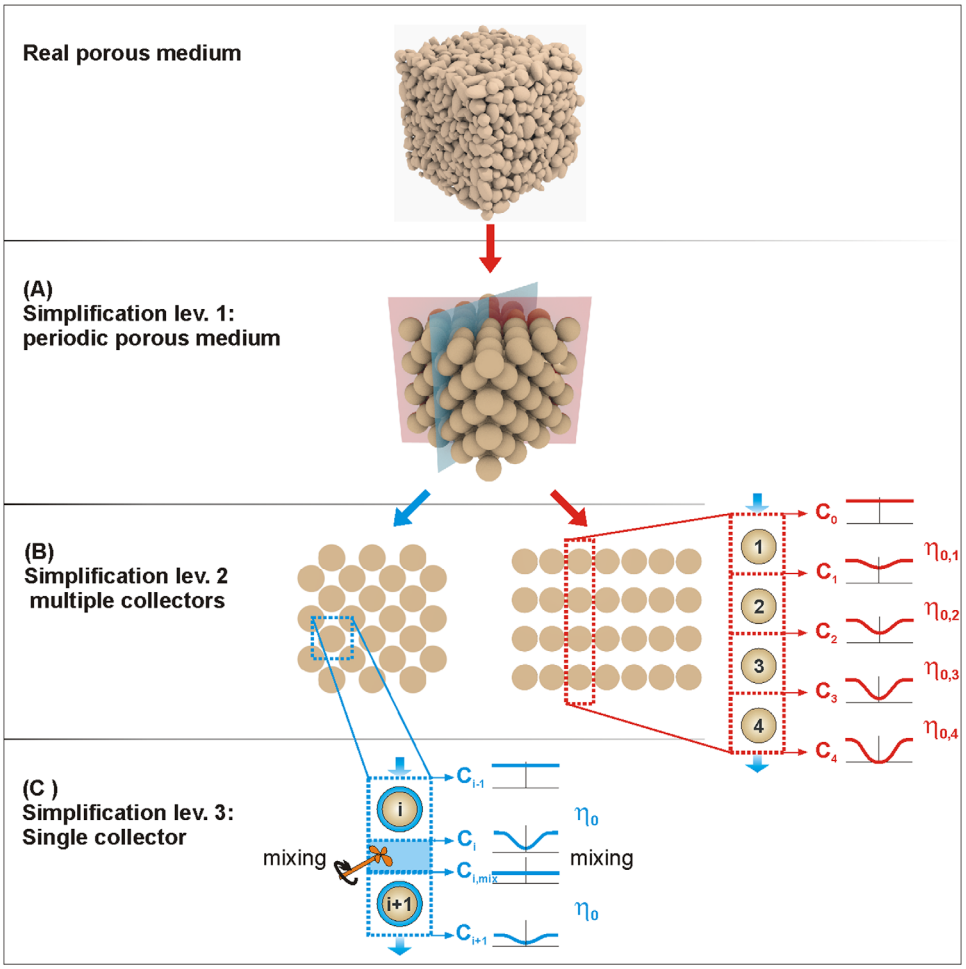

Figure 1. Conceptualization of real porous media: levels of simplification commonly adopted. (A) 3D periodic porous medium composed by identical spheres, (B) 2D representative sections, and (C) single collector.

between particles and porous medium (unfavorable deposition conditions). Under such circumstances, further removal mechanisms play a significant role (e.g., retention at grain-to-grain contacts) and may even dominate over the combined effects of advection, gravity, Brownian diffusion, and steric effect. In the cited work, the difference in removal efficiency between the first and deeper layers has been attributed to presence and absence of forward stagnation. This work aims at proving that under certain transport conditions, the approximation of uniform η may not be adequate even in the case of favorable deposition and that nonexponential profiles can be obtained also in the simplest case of favorable deposition. This hypothesis was supported by the results of this work analyzing the outcome from CFD particle transport simulations in the simplified porous medium composed by a vertical array of 50 identical spherical collectors, over a broad range of transport conditions (i.e., particle size, density, and flow rate).

2. Methods

2.1. Definition of Collector Efficiency for the Vertical Array

The model vertical array can be regarded as a discrete series of "unit collector cells" of length l along the flow direction, whose thickness depends on the porosity and pore space configuration [*Tien and Ramarao*, 2007]. N_c unit cells of length l are included in a porous medium of length L, being $L = l \cdot N_c$. At the steady state, the global efficiency (multiple collector efficiency) for a porous medium of length L can be calculated from the cumulated contribution of each collector encountered by the particles along the flow direction, following the general formulation proposed by *Tien and Ramarao* [2007]:

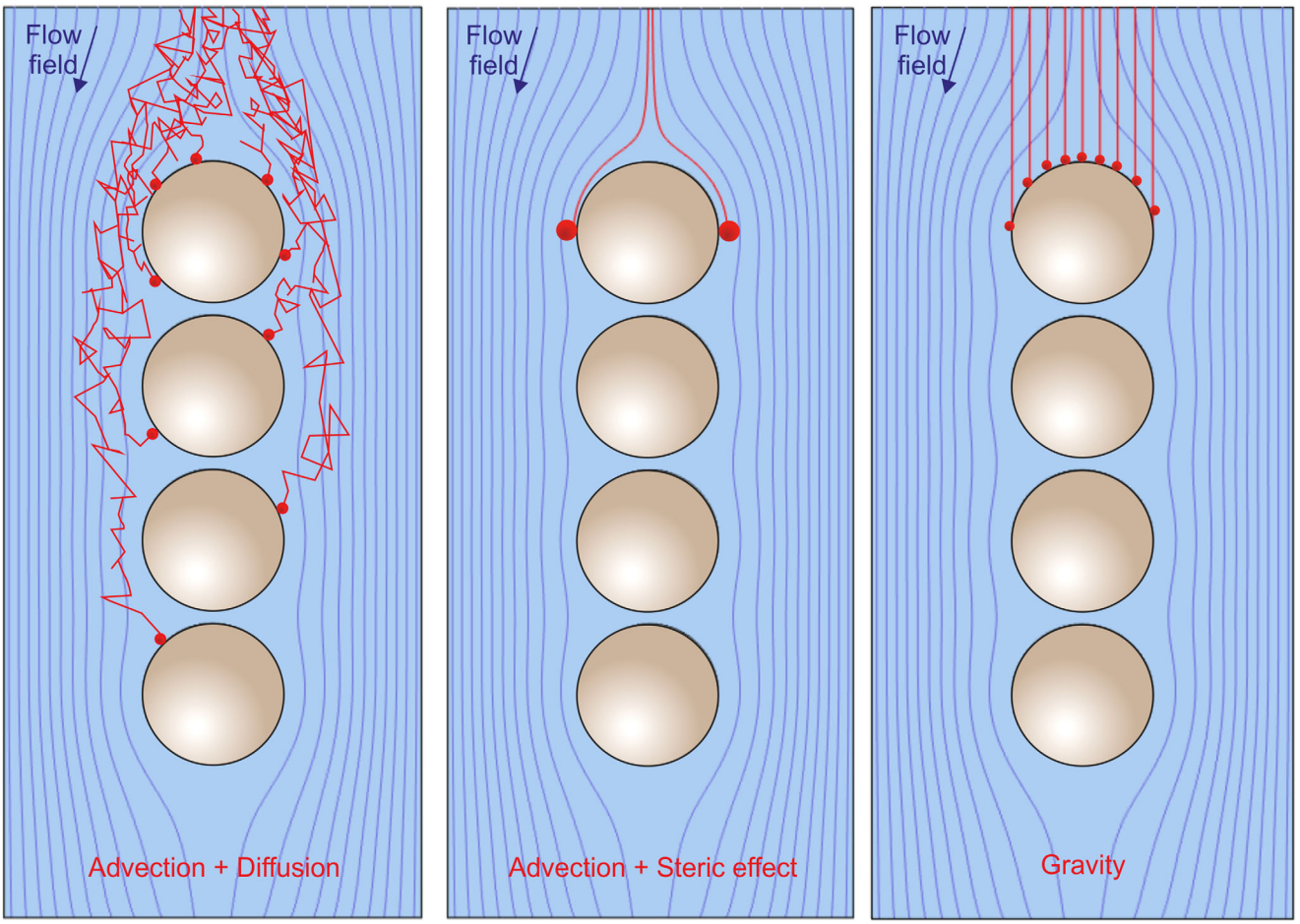

Figure 2. The main three mechanisms of deposition in case of multiple collectors in column: advection + Brownian diffusion (AD, usually referred to as Brownian diffusion, relevant for all collectors), advection + steric effect (AS, usually referred to as interception, relevant only for the first collector), and gravity (G, relevant only for the first collector).

$$E_{DM,N_c} = 1 - \frac{C_{DM,N_c}}{C_0} = 1 - \prod_{i=1}^{N_c} (1 - \eta_i), \tag{3}$$

where the subscript DM denotes the approach of a *discrete* series of N_c *multiple* collectors along the flow direction, and i counts the collectors (Figure 3A). Following this approach, the concentration in liquid phase and solid phase, C_{DM} and S_{DM} [ML^{-3}], are obtained from the equations reported in Table 1, first column (DM model). Flux-averaged concentrations are defined including all the transport mechanism as $C_i = \int_{A_i} (cu + cv - D\nabla c) \cdot ndA / \int_{A_i} u \cdot ndA$, where c is the (microscale) local concentration at section A_i, u is the (microscale) local advection velocity normal to section A_i, v is the gravity particle velocity normal to section A_i, D is the diffusion coefficient, and n is the versor normal to section A_i.

Under the approximation that the efficiency of the individual collectors is uniform within the packed bed, for a discrete series of N_c collectors the removal efficiency of the first collector of the series, η_1 (calculated as the removal efficiency of an isolated sphere), is extended to all collectors composing the porous medium. Under this hypothesis, equation (3) reduces to

$$E_{DS,N_c} = 1 - \frac{C_{DS,N_c}}{C_0} = 1 - (1 - \eta_1)^{N_c}, \tag{4}$$

where the subscript DS denotes the approach of a *discrete* series of *single* collectors (Figure 3B). Following this approach, the concentration in liquid phase and solid phase, C_{DS} and S_{DS}, are obtained from

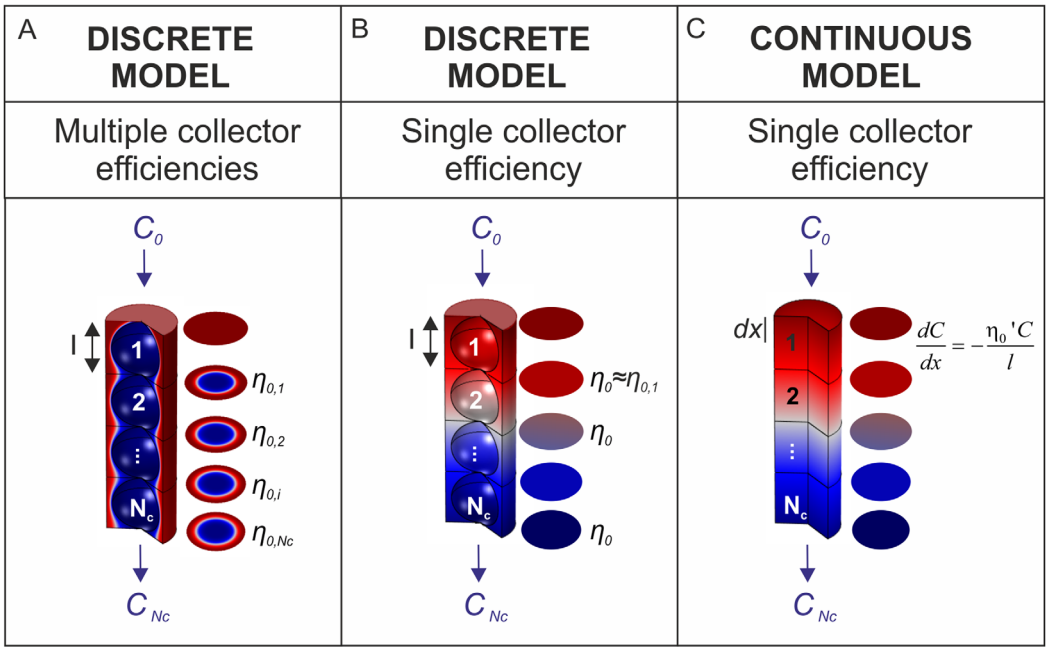

Figure 3. Porous medium configuration: continuous porous medium model and discrete series of collectors.

the equations reported in Table 1, second column (DS model), and exhibit an exponential decay over space.

More often, a simplified representation of the porous medium as a *continuum* is adopted, and a volume-averaging procedure is followed to derive the filter efficiency (Figure 3C). This procedure was introduced by *Friedlander* [1958] and applied by *Yao* [1968] to obtain the well-known formulation of removal efficiency in clean bed filtration under the assumption of uniform efficiency along the bed. The differential formulation of the concentration over space is therefore integrated along the filter length L, leading to the expressions reported in Table 1, third column (CS model) for the concentration in liquid phase and solid phase, C_{CS} and S_{CS}.

Table 1. Particle Concentration in Liquid and Solid Phase Obtained for the Discrete Model Using Multiple Collector Efficiency (DM Model), Discrete Model Using Single-Collector Efficiency (DS) and Continuous Model Using Single-Collector Efficiency (CS)[a]

		Discrete Model (DM) Multiple Collector Efficiency	Discrete Model (DS) Single-Collector Efficiency	Continuous Model (CS) Single-Collector Efficiency
Liquid phase	Single collector	$\frac{\Delta C_i}{\Delta x} = -\frac{\eta_{0,i}}{l} C_{i-1}$	$\frac{\Delta C_i}{\Delta x} = -\frac{\eta_{0,1}}{l} C_{i-1}$	$\frac{dC}{dx} = -\frac{\eta'_{0,1}}{l} C$
	First single collector, $x = l$	$\Delta C_1 = -\eta_{0,1} C_0$	$\Delta C_1 = -\eta_{0,1} C_0$	$\int_{C_0}^{C_1} \frac{dC}{C} = -\frac{\eta'_{0,1}}{l} \int_0^l dx$
		$\frac{C_1}{C_0} = 1 - \eta_{0,1}$	$\frac{C_1}{C_0} = 1 - \eta_{0,1}$	$\frac{C_1}{C_0} = \exp\left(-\eta'_{0,1}\right)$
	Array of collectors, $x = L = i \cdot l$	$E_i = 1 - \frac{C_i}{C_0}$ $\frac{C_i}{C_0} = \frac{C_1}{C_0} \cdot \frac{C_2}{C_1} \cdot \frac{C_3}{C_2} \cdot \ldots \cdot \frac{C_i}{C_{i-1}}$ $\frac{C_{DM,i}}{C_0} = \prod_{j=1}^{i} (1 - \eta_{0,j})$	$E_i = 1 - \frac{C_i}{C_0}$ $\frac{C_i}{C_0} = \frac{C_1}{C_0} \cdot \frac{C_2}{C_1} \cdot \frac{C_3}{C_2} \cdot \ldots \cdot \frac{C_i}{C_{i-1}}$ $\frac{C_{DS,i}}{C_0} = (1 - \eta_{0,1})^i$	$E_i = 1 - \frac{C_i}{C_0}$ $\int_{C_0}^{C_i} \frac{dC}{C} = -\frac{\eta'_{0,1}}{l} \int_0^L dx$ $\frac{C_{CS,i}}{C_0} = \exp\left(-i \cdot \eta'_{0,1}\right)$
Solid phase		$\frac{S_i}{C_0} = qt \frac{\eta_{0,i}}{l} \frac{C_{DM,i-1}}{C_0}$ $\frac{S_{DM,i}}{C_0} = qt \frac{\eta_{0,i}}{l} \prod_{j=1}^{i-1} (1 - \eta_{0,j})$	$\frac{S_i}{C_0} = qt \frac{\eta_{0,1}}{l} \frac{C_{DS,i-1}}{C_0}$ $\frac{S_{DS,i}}{C_0} = qt \frac{\eta_{0,1}}{l} (1 - \eta_{0,1})^{i-1}$	$\frac{S_i}{C_0} = qt \frac{\eta'_0}{l} \frac{C_{CS,i-1}}{C_0}$ $\frac{S_{CS,i}}{C_0} = qt \frac{\eta'_0}{l} \exp((i-1) \cdot \eta'_0)$

[a] η_0 and η_0' are the single-collector efficiency for the discrete and continuous porous medium model, respectively; C_0 and C_i are the concentration of suspended particles at the inlet and downstream the ith collector for unit of liquid volume, respectively; S_i is the concentration of retained particles on the ith collector for unit of total volume; L is the length of the porous medium; l is the length of a unit collector cell; x is the space variable aligned with the flow direction and q is the specific discharge rate (i.e., Q/A).

$$E_{CS,N_c} = 1 - \frac{C_{CS,N_c}}{C_0} = 1 - \exp\left(-N_c \eta'_1\right). \quad (5)$$

The original formulation of Yao [*Yao et al.*, 1971] is retrieved from equation (5) if the length of the unit collector l and the number of collectors N_c are expressed as a function of porosity and filter length, based on the geometry of the unit collector [*Tien and Ramarao*, 2007].

Equations (4) and (5) coincide when the efficiency η'_1 is related to the discrete η_1 by the expression

$$\eta'_1 = -\ln\left(1 - \eta_1\right). \quad (6)$$

2.2. Governing Equations and Numerical Simulations

The flow and particle transport simulations were run with the finite-elements software COMSOL Multiphysics®.

A simplified domain consisting of a vertical array of 50 cylindrical cells, each containing one spherical collector, was considered (Figure 4). A premixing and a postmixing zone were also included in the model domain in order to avoid the effect on boundary condition on the spheres. The length of the premixing and postmixing zones has been chosen in order to allow the flow field and the mass transfer boundary layer to completely develop within the domain. Sphere radius $a_c = 250$ μm, separation distance between spheres of 5 μm ($0.02 \cdot a_c$), and length of the premixing and postmixing zones of 3.75 mm ($15 \cdot a_c$) were used, thus resulting in a length of the unit collectors cells of 1.02 $a_c = 255$ μm. The radius of the cylindrical domain was imposed equal to $(1 + K) \cdot a_c$, where K is an adjustable coefficient, used to investigate different values of porosity. Due to the configuration of the model domain, porosity varies in the range 0.5–0.73, which are quite unusual of natural porous media, but may be representative of strung porous media [*Johnson and Hilpert*, 2013] and of packed beds used in industrial filtration [see, e.g., *Wakeman and Tarleton*, 2005]. The presented geometry, as well as the Happel's geometry, allows considering the effect of the neighborhood collectors on the flow field. Moreover, it is possible to analyze the concentration distribution between the series of spherical collectors and, therefore, to investigate the interference of subsequent collectors on particle transport.

The study was performed aligning flow and gravity fields as in most of the previous studies. In case of horizontal flow field and vertical gravity field, the simulation is no longer axial symmetric and the problem becomes more complicated, as discussed in some recent studies [*Chrysikopoulos and Syngouna*, 2014; *Syngouna and Chrysikopoulos*, 2016].

A broad range of conditions was investigated by performing a parametric sweep on flow velocity, particle size, particle density, and porosity. In particular, three values of porosity (0.50, 0.63, and 0.73) and flow velocity (10^{-7}, 10^{-6}, and 10^{-4} m/s) were considered. The explored conditions correspond to Peclet number in the range 0–2.37×10^5, gravity number in the range 0–1.48×10^2, and aspect ratio in the range 0–10^{-1}, covering most conditions relevant to filtration processes. An aspect ratio number equal to zero corresponds to the simulations in which the steric effect has not been considered. A detailed list of simulations and parameter values is reported in Table S1 in Supporting Information.

Meshing was performed by using triangular elements, except for the boundary layers close to the collectors, where a mesh refinement with quadrilateral elements was adopted. Since the critical value of the mass transfer boundary layer is in the order of hundreds of nm, a mesh composed by 100 layers, each 10 nm thick, was imposed around the spheres. Stokes flow field was solved by imposing nonslip boundary conditions on the surface of each collector, assigned vertical component of the velocity U at the inlet of the domain (at the top) and zero pressure at the outlet of the domain (at the bottom). Symmetry boundary condition was used at the lateral side of the domain. An example of model results is reported in Figure 4.

The particle transport was investigated performing both Lagrangian and Eulerian simulations at steady state. The Eulerian approach was adopted for those simulations including Brownian diffusion, solving the advective-diffusion equation. An inlet boundary condition of constant concentration C_0 was applied. Zero concentration was imposed on the grain surface (or at distance from the surface of the spheres equal to the particle radius in order to account for the steric effect) to simulate a perfect sink scenario. For simulations without diffusion, the Lagrangian approach was adopted and the trajectory analysis [*Rajagopalan and Tien*,

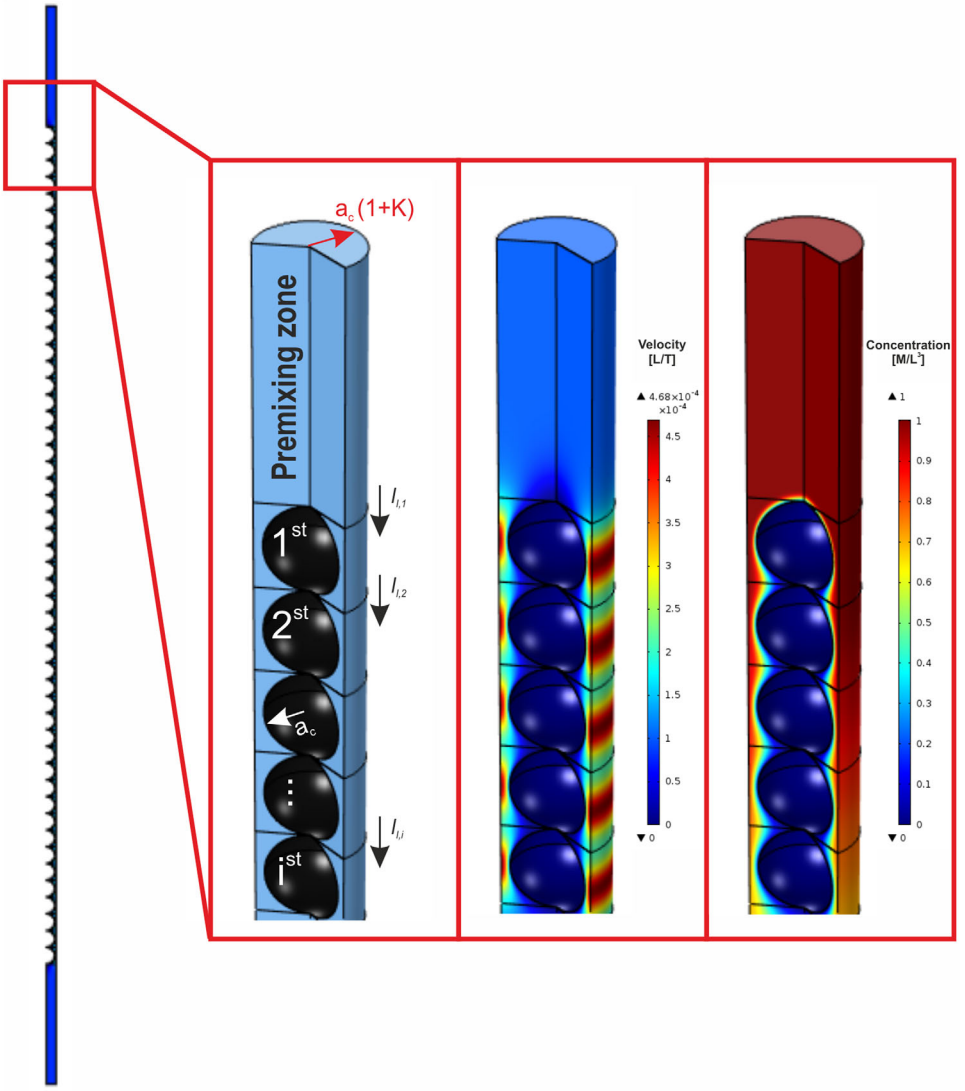

Figure 4. The investigated geometry (2D axial symmetrical) and 3D example results of the flow field velocity and concentration.

1976] was applied to calculate the flux of deposited particles. Further details on the approach adopted for the numerical simulations can be found in *Messina et al*. [2015].

The removal efficiency of the individual collectors $\eta_{i,CFD}$ in the array was calculated from the CFD results: the efficiency is obtained normalizing the flux of deposited particles by the total flux entering the unit collector cell (i.e., flux due to advection, gravity, and diffusion)

$$\eta_{i,CFD} = \frac{I_{s,i}}{I_{i-1}} = 1 - \frac{I_i}{I_{i-1}} = 1 - \frac{C_i qA}{C_{i-1} qA}, \tag{7}$$

where $I_{s,i}$ is the total flux of particles deposited on the ith sphere [MT^{-1}], I_{i-1} is the total flux approaching the ith sphere, and I_i is the total flux downstream the ith sphere, C_{i-1} is the total flux normalized concentration approaching the ith sphere [ML^{-3}], i.e., the ratio between the total particle flux and the water flux through the same section qA, and C_i is the total flux normalized concentration downstream the ith sphere [ML^{-3}]. This definition was adopted to avoid efficiency values greater than one which can be retrieved

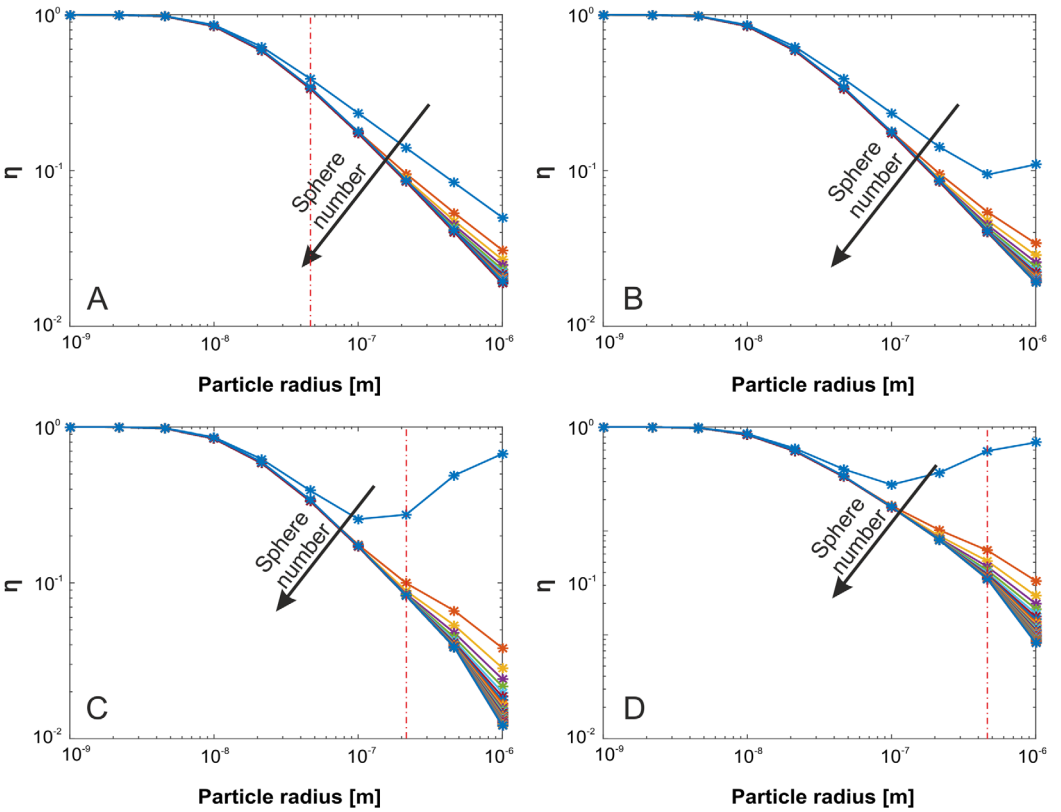

Figure 5. Single-collector efficiencies as a function of particle radius for $a_c = 250$ μm, $U = 10^{-6}$ m/s, $n = 0.5$, $\rho_f = 998$ kg/m^3, and particle density ρ_p = (A) 998 kg/m^3, (B) 1050 kg/m^3, (C) 4500 kg/m^3, (D) 7800 kg/m^3. The vertical red lines correspond to the three cases reported in Figures 7 and 8.

under specific conditions when applying the classical formulation of η_0 (i.e., normalized to the advective flux through the collector projection) [*Ma et al.*, 2013; *Nelson and Ginn*, 2011; *Song and Elimelech*, 1992], as discussed in details in *Messina et al.* [2015].

The concentration of particles retained onto the collectors, $S_{i,CFD}$, was calculated from $C_{i,CFD}$ using the equation of Table 1 for the DM model.

3. Results and Discussion

3.1. Collector Efficiency of Individual Spheres in the Array

The results of the transport simulations were processed first to calculate the removal efficiency of the individual spheres. Figure 5 reports the efficiency of each collector $\eta_{i,CFD}$ as a function of particle size for velocity $U = 10^{-6}$ m/s, a typical value encountered in fine sandy aquifers with limited gradients. Four values of particle density were considered, ranging from water density (Figure 5A, representative for example of viruses and bacteria) to density of bulk iron (Figure 5D, representative for example of nanoscale zerovalent iron particles used in groundwater remediation). Figure 6 reports the same results obtained at a higher velocity $U = 10^{-4}$ m/s, representative of natural flow conditions in sandy aquifer at intermediate hydraulic gradients (e.g., most alluvial aquifers in Centre and South Europe). The results for U = 10^{-7} m/s are reported in Supporting Information.

The trends of collector efficiency reported in Figure 5 immediately suggest that $\eta_{i,CFD}$ cannot be assumed uniform along the array of collectors, even in the presence of the favorable deposition conditions herein explored. Similar results are also found at higher velocities (Figure 6). For all particle size and density, the collector efficiency decreases with increasing distance from the inlet. In particular, particle removal occurs primarily on the first collector, which consequently has the highest efficiency. This difference is more pronounced when gravity

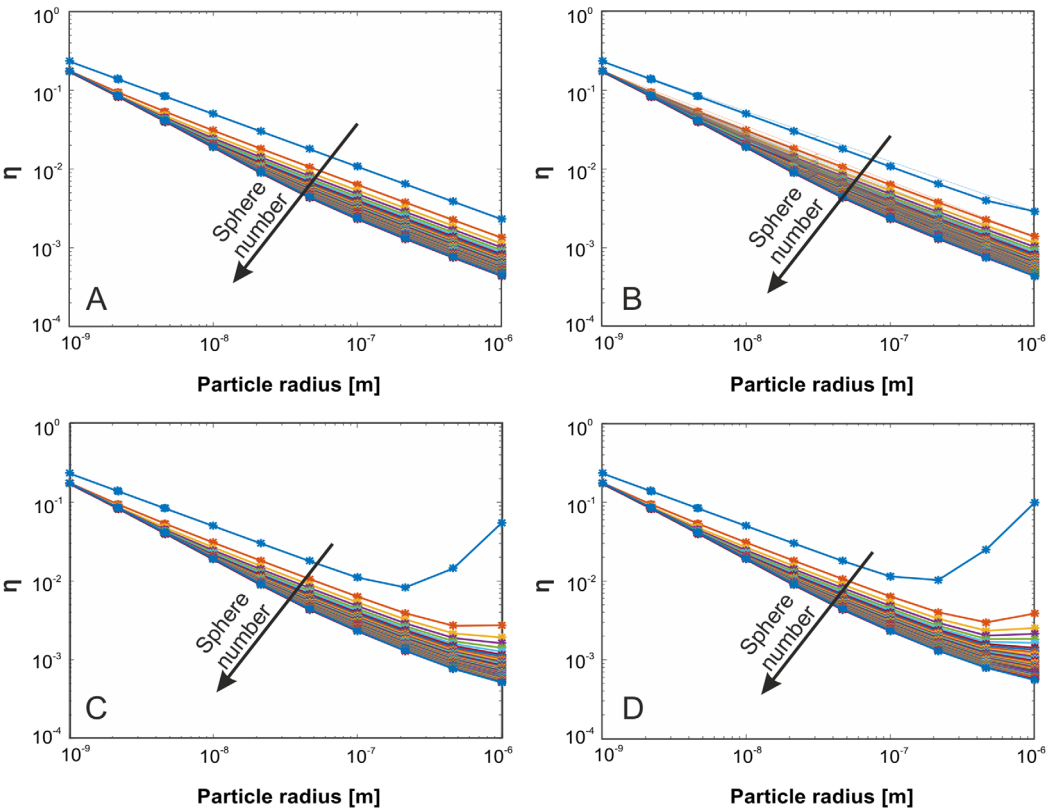

Figure 6. Single-collector efficiencies as a function of particle radius for $a_c = 250$ μm, $U = 10^{-4}$ m/s, $n = 0.5$, $\rho_f = 998$ kg/m^3, and particle density ρ_p = (A) 998 kg/m$_3$, (B) 1050 kg/m^3, (C) 4500 kg/m^3, (D) 7800 kg/m^3.

and/or interception are the predominant mechanisms, i.e., for large and heavy particles (cases C and D in Figures 5 and 6). Conversely, for small particles, whose deposition is primarily controlled by the combination of advection and Brownian diffusion (AD mechanism in Figure 3), density does not play a relevant role, and the collector efficiency does not change significantly with increasing distance from the inlet of the domain. In these cases, the approximation of collector efficiency $\eta_{i,CFD}$ being uniform along the array of collectors may be appropriate, and equation (4) could be applied for the upscaling to the column efficiency. In all other cases, on the contrary, variations of collector efficiency along the array cannot be neglected, and the column efficiency is to be calculated using the general formulation of equation (3).

Simulations reported in Figures 5 and 6 were obtained for a fixed spacing (5 μm) between spheres. Selected simulations (data not shown) were also performed in vertical arrays with larger distance between adjacent collectors, showing a substantial independence of the trends of removal efficiency on the spacing between spheres.

The numerical simulation results also confirm that as already observed qualitatively in section 1, for the first sphere of the array all removal mechanisms are important, while for the other spheres of the array deposition is predominantly due to the combined effect of advection and Brownian diffusion. The marked decrease in $\eta_{i,CFD}$ with increasing distance from the inlet can be associated to the relative importance of sedimentation and/or interception compared to the other removal mechanisms. If they dominate, the concentration profile downstream the first sphere is highly nonuniform with increasing radial distance. Increasing the size of the particles, the limited importance of Brownian diffusion does not allow a (at least partial) mixing between adjacent spheres, thus resulting in a significantly reduced removal on the second collector. This effect is progressively smoothed when passing to the following spheres, until an asymptotic, low removal efficiency is obtained far from the inlet of the domain (refer to Figure S4 in Supporting Information for further information on how the concentration profile changes along the collector radius).

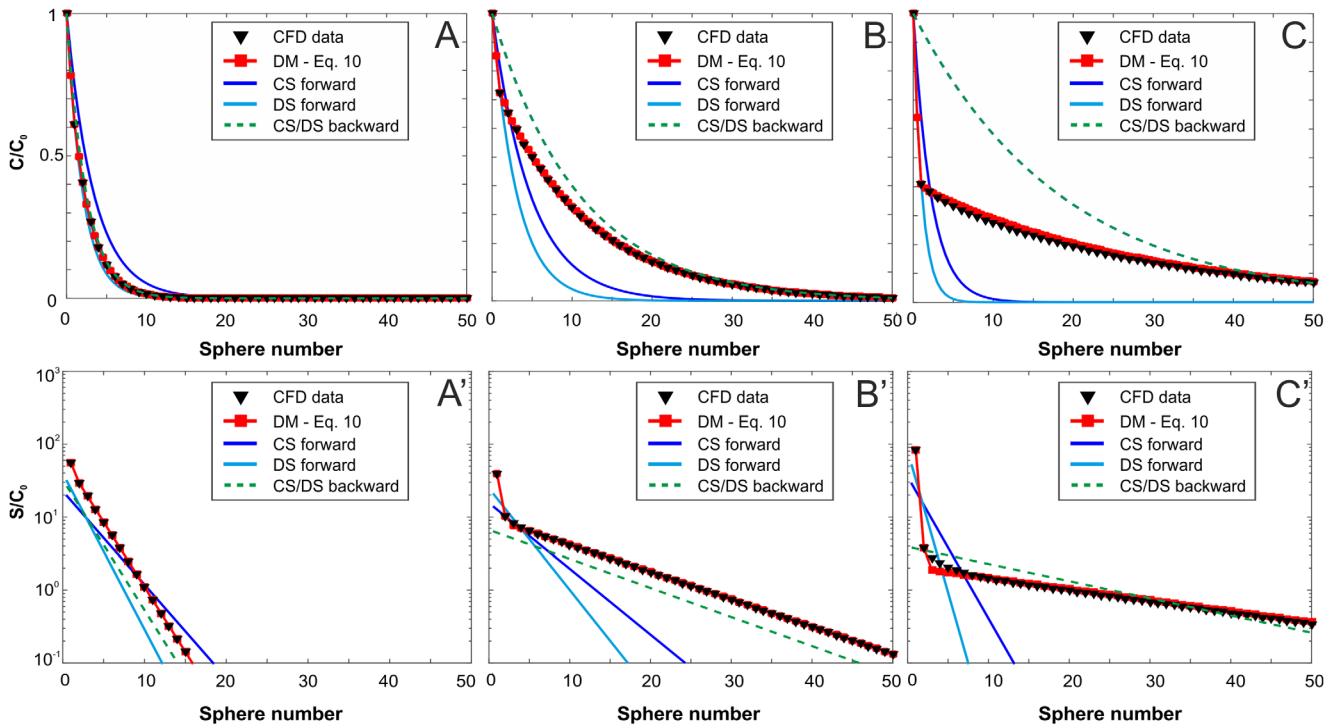

Figure 7. Normalized concentration in the liquid phase (A–C) and concentration at the solid phase evaluated after 20 h, normalized with respect to the total volume (A′, B′, and C′). The graphs report the CFD results in terms of $C_{i,CFD}$ and $S_{i,CFD}$ (black triangles), the concentration values predicted by direct application of the newly proposed DM model of equation (11) (in red), the CS model (in blue), and DS model (in light blues), and the concentration values obtained from the backward application of the DS and CS models to CFD results (in dotted green line). The simulations were run for: $a_p = 4.64 \times 10^{-8}$ m and $\rho_p = 998$ kg/m (A and A′); $a_p = 2.15 \times 10^{-7}$ m and $\rho_p = 4500$ kg/m^3 (B and B′); $a_p = 4.64 \times 10^{-7}$ m and $\rho_p = 7800$ kg/m^3 (C and C′). The reported results are obtained for $U = 10^{-6}$ m/s and $n = 0.50$.

In case gravity is not relevant (Figures 5A and 6A), for large particles (i.e., $a_p = 1$ μm) the difference in $\eta_{i,CFD}$ along the array can be attributed to the importance of the combined advection + steric effect (AS) as a removal mechanism.

3.2. Upscaling to Column Efficiency

The results of the CFD simulations were analyzed in terms of concentration profiles (suspended and attached) along the sphere array for different particle densities (Figure 7). The profiles show an exponential decay over distance for the A+A′ case (particles having the same density as water), as evidenced in particular by the plot of the solid phase concentration in the semilog graph. However, when increasing the density of the particles (and consequently the importance of sedimentation as a removal mechanism), the profiles become clearly nonexponential. In particular, in cases B+B′ and C+C′ the concentration profiles show a nonexponential trend for the first spheres of the array, while an exponential trend is observed for longer distances from the inlet. This finding suggests that the removal efficiency of the first sphere(s) is significantly different from those of the following ones, while an (almost) uniform removal efficiency is retrieved at longer distances from the inlet of the array, as qualitatively already observed in the previous paragraph.

The results of the CFD simulations were then compared to trends simulated using the DS and CS models of Table 1, both based on the assumption of uniform efficiency within the bed, and consequently providing exponential profiles in liquid and solid phase. The concentration profiles obtained for the DS and CS models were first calculated in forward mode, that is, assuming that the removal efficiency of the first sphere (η_1 and η'_1, respectively) applied to the entire porous medium (curves labeled as "DS forward" and "CS forward" in the figure). The graphs highlight that the trends predicted by the two models significantly deviate from the CFD results, particularly when the density contrast between particles and fluid is relevant (B+B′ and C+C′). Only moderate deviations are observed when particles have the same density as the fluid (A+A′).

Table 2. Values of η_1, η_2, and η_A Obtained From CFD Results and Values of η_{Fit} and η'_{Fit} Evaluated With Equation (8) for the Three Simulation Cases Reported Also in Figures 7 and 8

Simulations	η_1	η_2	η_A	η_{Fit}	η'_{Fit}
Case A $a_p = 4.64 \times 10^{-8}$ m, $\rho_p = 998$ kg/m	0.3891	0.3365	0.3362	0.3374	0.4115
Case B $a_p = 2.15 \times 10^{-7}$ m, $\rho_p = 4500$ kg/m^3	0.2743	0.0996	0.0827	0.0876	0.0917
Case C $a_p = 4.64 \times 10^{-7}$ m, $\rho_p = 7800$ kg/m^3	0.5903	0.0648	0.0343	0.0527	0.0542

The DS and CS models were then applied in backward mode to the CFD-simulated concentrations (curves labeled as "DS/CS backward"), following the approach commonly adopted when interpreting experimental concentration profiles retrieved from column transport tests: the concentrations at the model outlet $C_{Nc,CFD}$ were used to derive the column efficiencies as

$$\begin{cases} \eta_{Fit} = 1 - \left(\dfrac{C_{CFD,N_c}}{C_0}\right)^{1/N_c} \\ \eta'_{Fit} = -\dfrac{1}{N_c} \ln\left(\dfrac{C_{CFD,N_c}}{C_0}\right) \end{cases}. \quad (8)$$

The fitted efficiency values η_{Fit} and η'_{Fit}, which are related via equation (6), are significantly lower than the efficiency of the first sphere η_1, and much closer to the asymptotic efficiency of the array η_A (Table 2). Figure 7 shows that the fitted curves were not able to capture the trend of the CFD results. If the CFD-derived concentration profiles have been experimental data, the discrepancy between η_{Fit} (or η'_{Fit}) and η_0 of the single collector (in our case, the first collector of the array, therefore η_1) would have been (incorrectly) attributed solely to unfavorable attachment, to ripening or retention associated to grain-to-grain contact phenomena lumped into an attachment efficiency $\alpha < 1$, even in this case of favorable deposition conditions. Conversely, the simulation results here suggest that this deviation can also be partially attributed to nonuniform deposition induced by gravity and interception within a porous medium.

Based on these observations, a new model for the description of the removal efficiency along the column of collectors was derived. For a given simulation, the efficiencies $\eta_{i,CFD}$ decrease along the column (Figure 8). A quick drop is first observed at the first spheres, followed by a slow decrease down to an asymptotic value. For particles having the same density as the fluid (red curve in Figure 8, corresponding to A+A′ in Figure 7), an almost uniform efficiency is observed along the sphere array, except for the first collector. Conversely, for heavier particles (blue and green curves in Figure 8, corresponding to simulations B+B′ and C+C′ in Figure 7), an abrupt drop in efficiency is observed between the first and second collector, followed by a more smoothed decrease down to an asymptotic value.

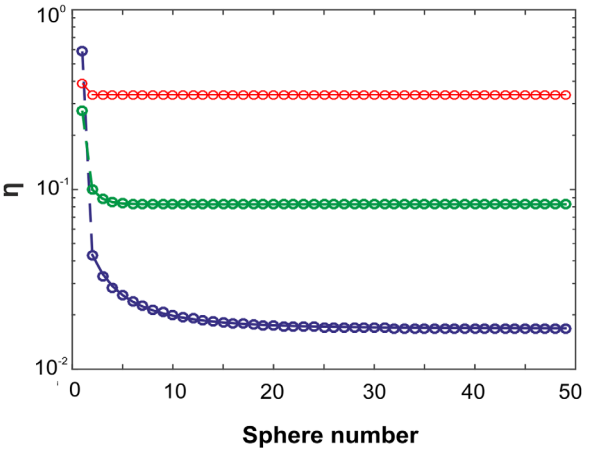

Figure 8. Example of trend of collector efficiency η_i as function of the sphere number. Points represent the CFD results, and lines are the corresponding efficiency trend modeled using equation (9). Data: $U = 10^{-6}$ m/s, $n = 0.50$, $a_p = 4.64 \times 10^{-8}$ m and $\rho_p = 998$ kg/m^3 (red, corresponding to A+A′ in Figure 7), $a_p = 2.15 \times 10^{-7}$ m and $\rho_p = 4500$ kg/m^3 (green, corresponding to B+B′ in Figure 7), $a_p = 4.64 \times 10^{-7}$ and $\rho_p = 7800$ kg/m^3 (blue, corresponding to C+C′ in Figure 7).

Starting from the second sphere, the efficiency trend ($\eta_2 \ldots \eta_{Nc}$) versus i can be described by an exponential relationship

$$\eta_i = (\eta_2 - \eta_A)\, \exp\left[\beta \cdot (2^{\delta} - i^{\delta})\right] + \eta_A, \quad (9)$$

where β and δ are fitting parameters controlling the shape of the curve, η_2 is the removal

efficiency of the second sphere, and η_A is the removal efficiency of the last sphere, corresponding to the asymptotic removal efficiency at large distances from the column inlet. For each CFD simulation, the single-collector efficiencies $\eta_{2,CFD} \ldots \eta_{Nc-1,CFD}$ were inverse-fitted to equation (9), neglecting the first sphere, thus determining β and δ. Solid lines in Figure 8 report the least squares fitted model of equation (9). By substituting equation (9) into equation (3), the following expression is obtained:

$$E = 1-(1-\eta_1)\prod_{i=2}^{N_c}\left[1-(\eta_2-\eta_A)\exp\left[\beta\cdot\left(2^{\delta}-i^{\delta}\right)\right]-\eta_A\right]. \quad (10)$$

Equation (10) is still too complex to be used to evaluate the efficiency of an entire system. Therefore, we can approximate the efficiency of each sphere, except those of the first two, with the asymptotic value η_A, and equation (10) becomes

$$E = 1-(1-\eta_1)(1-\eta_2)(1-\eta_A)^{N_c-2}. \quad (11)$$

This means that in order to describe the behavior of the entire array of collectors, at least three values of efficiency are to be evaluated (η_1, η_2, and η_A), not only one as usually done ($\eta_1 = \eta_{l0}$). Three flux-normalized correlation equations have been formulated to evaluate η_1, η_2, and η_A by performing a global fitting on all the numerical results and by taking into account all possible deposition mechanisms and mutual interactions, following the approach proposed by *Messina et al.* [2015]. The three complete models of η_1, η_2, and η_A, the corresponding calibration plot diagrams and their trend in realistic cases are reported in Supporting Information. The simulation results suggest that the relationship $\eta_1 > \eta_2 > \eta_A$ is always valid, as also inferable from the data reported in Table 2. Moreover, the values of η_{Fit} and η'_{Fit} are always within η_1 and η_A.

Based on the results herein presented, it can be concluded that the common assumption of uniform removal efficiency along a filter is not accurate under several circumstances, particularly for large and/or heavy particles, when gravity and advection play an important role in particle removal. In those cases, the removal onto the first collectors of the porous medium is remarkably higher than removal in the deep bed. To quantify the importance of the phenomenon, the decrease in efficiency along the vertical array was reported as a function of a combination of Peclet and gravity numbers, $N_{Pe} + N_{Pe}{}^{*}N_G$, where the second term represents a Peclet number calculated with respect to sedimentation rate (compare definitions in Table S1 of Supporting Information). The plot (Figure S7 in Supporting Information) shows that the assumption of uniform removal efficiency along the array is an acceptable approximation only for $N_{Pe} + N_{Pe}{}^{*}N_G$ lower than few tens.

4. Conclusions

The present study indicates that when considering particle deposition in a packed bed, the removal efficiency may not be uniform along the filter, even in the case of favorable deposition onto ideal spherical collector. As a consequence, colloid transport is not independent of the history of transport, and the assumption of constant removal efficiency along the filter bed may be significantly inadequate even in simplified porous media. This finding has direct implications for the interpretation of experimental results of particle transport tests. Nonexponential profiles of retained concentration are observed in several experimental conditions, e.g., in the presence of ripening and retention at grain-to-grain contacts [*Bradford et al.*, 2007; *Jones and Su*, 2014; *Kretzschmar et al.*, 1999; *Li et al.*, 2006]. In this case, the deviation is usually entirely attributed to retention mechanisms other than those controlling favorable deposition. However, the present study shows that the nonexponential shape of particles deposits may also be partly attributed to the three major removal mechanisms, and this result may sum up with the effects of other retention processes.

The ordered array of collectors considered in this study is a conceptualization representing real porous media at different degrees of accuracy. It is a direct representation of industrial filters, and of processes occurring at the surface water-groundwater interface. Conversely, in a natural porous medium such as aquifer systems there is typically no evidence of a "first sphere." However, more general conclusions can be drawn from the findings herein discussed, which may apply to colloid transport studies in general.

When interpreting experimental data, the single-collector efficiency is usually calculated based on models provided by the literature, and then extended to the entire medium. Experimental results are typically fitted

to estimate a uniform value of η and the discrepancies between the fitted η and the theoretically estimated η_0 of the isolated collector are lumped into the attachment efficiency $\alpha = \eta/\eta_0$. Values of $\alpha < 1$ are expected for particle transport under unfavorable deposition conditions, when not all collisions result in attachment. However, some studies of particle transport reported attachment efficiency values lower than the unit also under favorable deposition conditions [*Foppen and Schijven*, 2005; *Pelley and Tufenkji*, 2008]. Such unexpected values of α can be attributed to other retention phenomena (e.g., surface heterogeneities, presence of adsorbed polymers, etc.). However, a possible additional contribution can be attributed to the simplifying assumption of uniform removal efficiency, equal to the removal efficiency of an isolated sphere, to the entire porous medium. In our study, we demonstrate that even in the simplest case of favorable deposition with no grain-to-grain contacts, the removal efficiency within bulk array of collectors, η_A, is lower than that of the first sphere, η_1. As a consequence, if the removal efficiency calculated for a single collector is directly applied to the "bulk" porous medium, this may lead to a significant overestimation of the actual removal efficiency, and consequently in the application of values of α significantly lower than one in order to get rid of this discrepancy.

Acknowledgments
The data for this paper are available by contacting the corresponding author.

References

Anders, R., and C. V. Chrysikopoulos (2005), Virus fate and transport during artificial recharge with recycled water, *Water Resour. Res.*, *41*, W10415, doi:10.1029/2004WR003419.

Bianchi Janetti, E., I. Dror, M. Riva, A. Guadagnini, X. Sanchez-Vila, and B. Berkowitz (2013), Mobility and interaction of heavy metals in a natural soil, *Transp. Porous Media*, *97*(3), 295–315.

Bradford, S. A., S. Torkzaban, and S. L. Walker (2007), Coupling of physical and chemical mechanisms of colloid straining in saturated porous media, *Water Res.*, *41*(13), 3012–3024.

Chrysikopoulos, C. V., and V. I. Syngouna (2014), Effect of gravity on colloid transport through water-saturated columns packed with glass beads: Modeling and experiments, *Environ. Sci. Technol.*, *48*(12), 6805–6813.

Cookson, J. T. (1970), Removal of submicron particles in packed beds, *Environ. Sci. Technol.*, *4*(2), 128–134.

Cushman, J. H., and T. R. Ginn (2000), Fractional advection-dispersion equation: A classical mass balance with convolution-Fickian flux, *Water Resour. Res.*, *36*(12), 3763–3766.

Elimelech, M., X. Jia, J. Gregory, and R. Williams (1995*), Particle Deposition and Aggregation: Measurement, Modelling, and Simulation*, 441 pp., Butterworth-Heinemann, Oxford, U. K.

Elimelech, M., X. Jia, J. Gregory, and R. Williams (1998), *Particle Deposition and Aggregation: Measurement, Modeling and Simulation*, 448 pp., Butterworth-Heinemann, Oxford, U. K.

Foppen, J. W. A., and J. F. Schijven (2005), Transport of *E. coli* in columns of geochemically heterogeneous sediment, *Water Res.*, *39*(13), 3082–3088.

Friedlander, S. K. (1958), Theory of aerosol filtration, *Ind. Eng. Chem.*, *50*(8), 1161–1164.

Happel, J. (1958), Viscous flow in multiparticle systems: Slow motion of fluids relative to beds of spherica particle, *AIChE J.*, *4*(2), 197–201.

Herzig, J. P., D. M. Leclerc, and P. L. Goff (1970), Flow of Suspensions through porous media—Application to deep filtration, *Ind. Eng. Chem.*, *62*(5), 8–35.

Iwasaki, T. (1937), Some notes on sand filtration, *Am. Water Works Assoc.*, *29*, 1591–1602.

Johnson, W. P., and M. Hilpert (2013), Upscaling colloid transport and retention under unfavorable conditions: Linking mass transfer to pore and grain topology, *Water Resour. Res.*, *49*, 5328–5341, doi:10.1002/wrcr.20433.

Jones, E. H., and C. Su (2014), Transport and retention of zinc oxide nanoparticles in porous media: Effects of natural organic matter versus natural organic ligands at circumneutral pH, *J. Hazard. Mater.*, *275*, 79–88.

Kretzschmar, R., M. Borkovec, D. Grolimund, and M. Elimelech (1999), Mobile subsurface colloids and their role in contaminant transport, *Adv. Agron.*, *66*, 121–193.

Le Borgne, T., D. Bolster, M. Dentz, P. DeAnna, and A. Tartakovsky (2011), Effective pore-scale dispersion upscaling with a correlated continuous time random walk approach, *Water Resour. Res.*, *47*(12), W12538.

Li, J., X. Xie, and S. Ghoshal (2015), Correlation equation for predicting the single-collector contact efficiency of colloids in a horizontal flow, *Langmuir*, *31*(26), 7210–7219.

Li, X., C. L. Lin, J. D. Miller, and W. P. Johnson (2006), Role of grain-to-grain contacts on profiles of retained colloids in porous media in the presence of an energy barrier to deposition, *Environ. Sci. Technol.*, *40*(12), 3769–3774.

Long, W., and M. Hilpert (2009), A correlation for the collector efficiency of Brownian particles in clean-bed filtration in sphere packings by a Lattice-Boltzmann method, *Environ. Sci. Technol.*, *43*(12), 4419–4424.

Ma, H. L., J. Pedel, P. Fife, and W. P. Johnson (2009), Hemispheres-in-cell geometry to predict colloid deposition in porous media, *Environ. Sci. Technol.*, *43*(22), 8573–8579.

Ma, H. L., M. Hradisky, and W. P. Johnson (2013), Extending applicability of correlation equations to predict colloidal retention in porous media at low fluid velocity, *Environ. Sci. Technol.*, *47*(5), 2272–2278.

McDowell-Boyer, L. M., J. R. Hunt, and N. Sitar (1986), Particle transport through porous media, *Water Resour. Res.*, *22*(13), 1901–1921.

Messina, F., D. L. Marchisio, and R. Sethi (2015), An extended and total flux normalized correlation equation for predicting single-collector efficiency, *J. Colloid Interface Sci.*, *446*, 185–193.

Molnar, I. L., W. P. Johnson, J. I. Gerhard, C. S. Willson, and D. M. O'Carroll (2015), Predicting colloid transport through saturated porous media: A critical review, *Water Resour Res.*, *51*, 6804–6845, doi:10.1002/2015WR017318.

Nelson, K. E., and T. R. Ginn (2011), New collector efficiency equation for colloid filtration in both natural and engineered flow conditions, *Water Resour. Res.*, *47*, W05543, doi:10.1029/2010WR009587.

Ngueleu, S. K., P. Grathwohl, and O. A. Cirpka (2014), Altered transport of lindane caused by the retention of natural particles in saturated porous media, *J. Contam. Hydrol.*, *162–163*, 47–63.

Pelley, A. J., and N. Tufenkji (2008), Effect of particle size and natural organic matter on the migration of nano- and microscale latex particles in saturated porous media, *J. Colloid Interface Sci.*, *321*(1), 74–83.
Petosa, A. R., D. P. Jaisi, I. R. Quevedo, M. Elimelech, and N. Tufenkji (2010), Aggregation and deposition of engineered nanomaterials in aquatic environments: Role of physicochemical interactions, *Environ. Sci. Technol.*, *44*(17), 6532–6549.
Rajagopalan, R., and C. Tien (1976), Trajectory analysis of deep-bed filtration with sphere-in-cell porous-media model, *AIChE J.*, *22*(3), 523–533.
Saleh, N., T. Phenrat, K. Sirk, B. Dufour, J. Ok, T. Sarbu, K. Matyiaszewski, R. D. Tilton, and G. V. Lowry (2005), Adsorbed triblock copolymers deliver reactive iron nanoparticles to the oil/water interface, *Nano Lett.*, *5*(12), 2489–2494.
Song, L. F., and M. Elimelech (1992), Deposition of Brownian particles in porous-media—Modified boundary-conditions for the sphere-in-cell model, *J. Colloid Interface Sci.*, *153*(1), 294–297.
Syngouna, V. I., and C. V. Chrysikopoulos (2013), Cotransport of clay colloids and viruses in water saturated porous media, *Colloids Surf. A*, *416*, 56–65.
Syngouna, V. I., and C. V. Chrysikopoulos (2016), Cotransport of clay colloids and viruses through water-saturated vertically oriented columns packed with glass beads: Gravity effects, *Sci. Total Environ.*, *545–546*, 210–218.
Tien, C., and A. C. Payatakes (1979), Advances in deep bed filtration, *AIChE J.*, *25*(5), 737–759.
Tien, C., and B. V. Ramarao (2007), *Granular filtration of aerosols and hydrosols*, Oxford, Elsevier.
Tiraferri, A., T. Tosco, and R. Sethi (2011), Transport and retention of microparticles in packed sand columns at low and intermediate ionic strengths: Experiments and mathematical modeling, *Environ. Earth Sci.*, *63*(4), 847–859.
Torkzaban, S., S. S. Tazehkand, S. L. Walker, and S. A. Bradford (2008), Transport and fate of bacteria in porous media: Coupled effects of chemical conditions and pore space geometry, *Water Resour. Res.*, *44*, W04403, doi:10.1029/2007WR006541.
Tosco, T., D. L. Marchisio, F. Lince, and R. Sethi (2013), Extension of the Darcy-Forchheimer law for shear-thinning fluids and validation via pore-scale flow simulations, *Transp. Porous Media*, *96*(1), 1–20.
Tosco, T., M. P. Papini, C. C. Viggi, and R. Sethi (2014), Nanoscale zerovalent iron particles for groundwater remediation: A review, *J. Cleaner Prod.*, *77*, 10–21.
Tufenkji, N., and M. Elimelech (2004), Correlation equation for predicting single-collector efficiency in physicochemical filtration in saturated porous media, *Environ. Sci. Technol.*, *38*(2), 529–536.
Wakeman, R. J., and E. S. Tarleton (2005), *Principles of Industrial Filtration*, 339 pp., Elsevier.
Yao, K. M. (1968), Influence of suspended particle size on the transport aspect of water filtration, PhD dissertation, Univ. of N. C. at Chapel Hill, Chapel Hill.
Yao, K. M., M. M. Habibian, and C. R. O'Melia (1971), Water and waste water filtration—Concepts and applications, *Environ. Sci. Technol.*, *5*(11), 1105–1112.
Zeinijahromi, A., A. Vaz, and P. Bedrikovetsky (2012), Well impairment by fines migration in gas fields, *J. Pet. Sci. Eng.*, *88–89*, 125–135.